Cold-Denatured Ensemble of Apomyoglobin: Implications for the Early Steps of Folding†

J. Sabelko, J. Ervin, and M. Gruebele*

School of Chemical Sciences and Beckman Institute for Advanced Science and Technology, University of Illinois, Urbana, Illinois 61801

Received: September 30, 1997; In Final Form: December 10, 1997

The dynamics of protein-refolding experiments initiated by a temperature jump depend critically on the nature of the initial cold-denatured ensemble. The cold-denatured state of *equine* apomyoglobin has been investigated in aqueous buffers by near- and far-UV circular dichroism, fluorescence, infrared, and NMR spectroscopies at temperatures ranging from −20 to 98 °C. Cold denaturation of apomyoglobin is well described by a cooperative transition below 3 °C and differs in many aspects from acid-induced unfolding. As a reference system, the N-terminal A-peptide fragment of *equine* apomyoglobin has also been studied in aqueous and trifluoroethanol solutions. The A-peptide has a low helix-forming propensity in the absence of any stabilizing tertiary interactions. The results show that cold denaturation breaks the AGH-hydrophobic interface of *equine* apomyoglobin. Furthermore, at least some GH-helical structure appears to be preserved at the expense of the less stable A-helix.

Introduction

Cold denaturation of the secondary and tertiary structure of proteins in aqueous solution is now a well-established fact.[1−5] It provides a convenient initial ensemble for refolding studies based on temperature jumps.[6] Backbone kinetics during refolding from a cold-denatured ensemble have been observed experimentally on microsecond[7] and even submicrosecond time scales.[8]

On the nanosecond time scale of fast temperature-jump experiments, the backbone structure cannot respond with large amplitude motions due to the large protein size and solvent viscosity.[9] The properties of the cold-denatured state therefore determine the starting ensemble of any folding processes following a temperature jump. In some pressure- and cold-denatured proteins, residual secondary or tertiary structure has been found to persist.[10] In other cases, especially in the presence of small concentrations of denaturants, complete loss of secondary structure has been reported.[4,11] The mechanism of cold denaturation evidently allows for a wide range of partially to wholly unfolded states.

There is direct experimental evidence for the nature of that mechanism. Solvated amino acid neutron diffraction[12] shows that water molecules are more ordered around hydrophobic than around hydrophilic residues, favoring solvation of hydrophilic residues. However, the solvent structure becomes more ordered at lower temperatures, finally allowing hydrophobic residues to be solvated without a large entropic cost. The extent to which core and secondary structure losses occur at experimentally reachable temperatures depends on the protein at hand. Supercooling allows access to temperatures as low as −20 °C in aqueous solution in the present work.

Several variants of apoMb are known to cold denature with a significant loss of secondary structure in an apparently cooperative two-state process.[6,13,14] Due to the differences between denaturation mechanisms, there is no intrinsic reason the cold-denatured state should particularly resemble ensembles resulting from heat, pH, or chemical denaturation. Indeed, our characterization by a variety of probes shows that it differs in significant aspects from other denatured states.

The experiments described here focus mainly on the AGH-hydrophobic core of *eq*-apoMb,[15] which in part or whole represents the most stable structure in the protein. All tryptophan residues are contained in the A-helix, while all tyrosine residues are contained in the GH-helices. This results in very specific probing by near-UV CD and fluorescence techniques, which we have supplemented by infrared and NMR spectroscopies. As a benchmark, the A-peptide has also been studied in aqueous and TFE solutions. Its folding propensity has been uncertain in the literature, although it clearly plays a critical role in the formation of the AGH-hydrophobic core. (The B-helix also plays a role in the full ABGH- core[15] but is probed by only a few data in the present work.)

Our results indicate that cold denaturation disrupts the AGH-core of *eq*-apoMb. Furthermore, A-peptide is found to have little helix-forming propensity, and the A-helix appears to significantly unfold upon cold denaturation of the whole protein. This leads to the construction of a pH/temperature "phase diagram" for residual structure in the A−(GH) core region of the protein.

In contrast, it is generally assumed in the literature that the AGH-core acts as a single unit during folding. This is based on data collected for sperm whale apomyoglobin (*physeter catodon*, *pc*-apoMb).[16−24] Our data suggests that there are significant differences in the folding behavior of *pc*- and *eq*-apoMb, *pc*-apoMb generally having a higher propensity for maintaining an intact AGH-core region. Sequence differences, particularly in the A-helix region of the proteins, also indicate that *pc*-apoMb may not be a "typical" representative of the mammalian apoMb family and that results from experiments on *pc*-apoMb cannot be compared with those on *eq*-apoMb without great caution.

† Abbreviations: Mb, myoglobin; apoMb, apomyoglobin; *pc*-, sperm-whale (*physeter catodon*); *eq*-, horse (*equus caballus*); I-state, acid intermediate; SVD, singular value decomposition; GuHCl, guanidinium hydrochloride; TFE, trifluoroethanol.

S1089-5647(97)03178-7 CCC: $15.00
Published on Web 02/14/1998

Figure 1. 3-D structure of horse apomyoglobin based on X-ray data of myoglobin and visualized using VMD.[51,73] NMR spectroscopy indicates an intact ABGH-core in the native state, as well as a BCD-core, while the E- and F-segments around the heme pocket apparently lose some structure. The tryptophan 7 and 14, tyrosine 103 and 146, and methionine 131 residues of importance in the text are highlighted.

In view of the results obtained here, previous kinetic experiments can be interpreted as a "half-collision" process,[8] during which the A-helix forms and condenses with the partially preexisting GH-complex to form the nativelike AGH-core in a few microseconds. In *eq*-apoMb, the A-helix folding propensity is sufficiently low that GH- and A-formation could be sequential processes, whereas in *pc*-apoMb, the greater stability of the A-helix, as well as previous studies,[23] indicate that the process may be kinetically more concerted.

Experimental Section

1. Samples and Handling. *Apomyoglobin.* The structure of *eq*-Mb is dominated by eight α-helices, A−H (Figure 1). Upon heme removal, several of the helices previously involved in heme binding lose helical structure, but the AGH-hydrophobic core looks much as it does in the native holoprotein.[15] The protein contains only two tryptophan residues, both located within the A-helix (positions 7 and 14) and two tyrosine residues located near the C-terminus of the H-helix (Y146) and at the GC-interface (Y103). A methionine residue (M131) is located in the H-helix and is almost in van der Waals contact with tryptophan 14 (W14).[15]

The AGH-hydrophobic core is particularly stable in some variants of apoMb. Amide protection factor measurements and site-directed mutagenesis studies on the *pc*-apoMb protein indicate that this core remains intact even in the pH 4.2 acid intermediate.[20−22] An AGH-core with protection factors up to 100 (compared to factors up to 200 000 in the native state) appears as a refolding intermediate following urea concentration jumps.[23] It is also a likely intermediate in submillisecond folding studies based on cold denaturation of *eq*-apoMb.[8] However, acid denaturation of *pc*-Mb indicates that GH alone may form a stabilized intermediate under certain conditions (S. A. Asher, in press), and the present work indicates that the *eq*-apoMb AGH-core is highly disrupted by cold denaturation.

Eq-apoMb was prepared via a modified acid−acetone extraction method using *eq*-Mb purchased from Sigma without any further purification.[25] After the initial extraction, the protein was rinsed in −20 °C acetone, centrifuged, and air-dried before being redissolved in H_2O and lyophilized. Lyophilized protein was stored at −20 °C until needed. If experiments were to be performed in D_2O, the protein was dissolved in unbuffered D_2O, allowed to exchange for a few hours, and then lyophilized again. This cycle was repeated 1−3 times. Buffering and concentration conditions are reported with each experiment. pH was measured at each particular concentration at room temperature after protein addition. In D_2O solutions pH was not corrected for the isotope effect and will be reported as pH*.

Apoprotein concentrations were determined by UV/vis spectroscopy as described by Edelhoch[26] using extinction coefficients of 13 940 M^{-1} cm^{-1} and 15 220 M^{-1} cm^{-1} for wild-type *eq*-apoMb and *pc*-apoMb, respectively. *eq*-Mb concentrations were determined using the Soret band at 409 nm and the extinction coefficient (175 ± 11 mM^{-1} cm^{-1}) averaged over three literature values and our own determination from weighed lyophilized protein.[27−29] Heme contamination of the apo-protein was found to be less than 1% for all samples.

M131A *pc*-apoMb was provided by M. Kay and R. Baldwin.[22] Plasmid pMb122 containing a synthetic gene for *pc*-Mb was provided by S. Sligar, and the protein was overexpressed in *Escherichia coli* strain TB-1.[30] Cultures were grown in LB containing 200 mg/L ampicillin for 18−24 h before being centrifuged and stored at −70 °C for later use. Cells were lysed using a cell disrupter and centrifuged for 30 min at 30 000 rpm in a Beckman Ti45 rotor. The supernatant was adjusted to pH 5.9 and loaded on a CM-52 ion exchange column preequilibrated with pH 6.0, 10 mM phosphate. The protein was eluted using a pH gradient, and the primary myoglobin containing fractions were pooled and concentrated using an Amicon pressure cell and YM10 membrane. Heme extraction, lyophilization, and protein storage were carried out as described above.

A-peptide. A-peptide, residues 1−18 of *eq*-apoMb, was synthesized by standard Fmoc protected, solid-phase methods at the University of Illinois Biotechnology Lab. Purified by reverse-phase C_{18} HPLC, the peptide had >90% purity as shown by analytical HPLC. Its molecular weight was confirmed by ES-MS. The A-peptide had free carboxyl and amino ends and corresponds directly to the first two amino-terminal residues plus A-helix in the native protein. Its sequence

H Gly Leu Ser Asp Gly Glu Trp Gln Gln Val Leu Asn
Val Trp Gly Lys Val Glu OH

differs from that of the corresponding *pc*-apoMb segment at residue positions 1 (Val for Gly), 4 (Glu for Asp), 9 (Leu for Gln), 12 (His for Asn), and 15 (Ala for Gly), giving a fairly low 72% homology compared to >90% for both the G- and H-helices.

The A-peptide proved to be only marginally soluble in 40 mM phosphate buffer, restricting peptide concentrations, in the absence of TFE, to 20 μM and under. Sample concentrations were measured using the absorbance at 280 nm with an extinction coefficient of 11 200 M^{-1} cm^{-1},[32] all were filtered (0.2 μm) before use, and ellipticity at 222 nm showed a linear dependence on concentration between 2 and 20 μM. For NMR experiments on A-peptide, deuterated TFE addition allowed for concentrations in excess of 100 μM.

Supercooling. Cold denaturation was monitored to temperatures as low as −20 °C in supercooled aqueous solutions. To minimize the effective freezing temperature, as many potential nucleation sites as possible were eliminated through a combination of 0.22-μm filtering, vacuum degassing, and judicious choice of sample cells. Sample cells must be designed to avoid

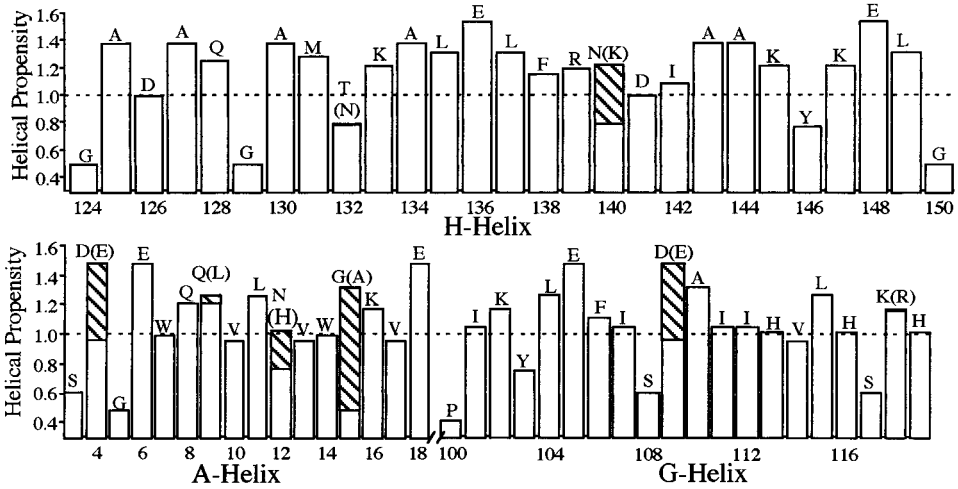

Figure 2. Plot of residue number versus its helical propensity based on Williams et al.[37] Letters indicate the amino acid at each residue position for *eq*-apoMb. Residues that are different in the sperm whale protein are shown in parentheses and are stabilizing in every case except for residue 118, where the substitution is neutral (crosshatches). While G and H show high homology, the A-helix of *eq*-apoMb has considerably less helical propensity.

the introduction of any possible nucleation sites, thereby prohibiting the use of most commercial fluorescence and CD cells comprised of fused quartz plates, which typically have small defects and could be consistently cooled to only −7 °C. The use of extruded synthetic quartz cells significantly increased the range of accessible temperatures. In particular, flame annealed and sealed 0.3 mm × 3.0 mm synthetic quartz capillary tubes (VitroCom) were used for most subzero CD and fluorescence measurements and typically allowed cooling below −15 °C before freezing.

Concentration Effects and Aggregation. Aggregation of proteins could affect their folding characteristics and must be kept to a minimum. Recently it has been shown that an aggregation artifact could have been easily mistaken for an intermediate in a mutant of human spliceosomal protein.[31] With this in mind, a series of fluorescence measurements were performed on *eq*-apoMb at pH 5.9 in 40 mM phosphate buffer over a concentration range from 10 to 200 μM. The data showed no significant changes in the concentration-scaled spectral shape. Likewise, a series of far-UV CD spectra taken over a concentration range from 3 to 50 μM also showed no significant variation in their mean residue ellipticities.

Temperature-scanned CD spectra in the −8 to 15 °C range showed that cold denaturation was reversible within <5% over periods ranging from minutes to several hours. One would generally expect cold-denaured proteins to be considerably less susceptible to irreversible aggregation than heat-denatured proteins, due to the weakened hydrophobic interaction at low temperatures. For example, in 1.5 mM solutions of *eq*-apoMb filtered with a 200-nm filter, no visible precipitation of protein is observed over a period of at least 4 h at 0 °C, while a precipitate forms in less than 1 h at room temperature.

NMR spectra of apoMb were taken at pH* 5.9 at concentrations up to 1.5 mM to check for aggregation. Below 700 μM, samples showed none of the typical signs of aggregation (e.g., precipitation) at room temperature or following extended periods at −8 °C, and the spectra displayed concentration-independent line widths. However, room-temperature *eq*-apoMb NMR spectra taken at concentrations exceeding 1.5 mM show simplification and broadening of their downfield regions, while their far upfield regions remain qualitatively similar. Exactly this would be expected for an aggregating protein. The far-upfield resonances correspond to protons buried within the protein's hydrophobic core and should not be severely affected by aggregation, while the resonances between 7.9 and 8.5 ppm, primarily histidine C^{ϵ} resonances,[15] which are often found to be solvent exposed in the apoMb protein, should be most affected by the aggregation of protein exteriors. All NMR experiments reported here were therefore taken at concentrations below 700 μM.

2. A-peptide Reference. Microcalorimetric measurements show that the standard heat capacity (ΔC_p^{cd}) of apomyoglobin increases upon transition from the native to the cold-denatured state.[14] A positive ΔC_p^{cd} indicates exposure of hydrophobic surface area to water and strongly suggests that cold denaturation involves solvation of the protein's hydrophobic core. This mechanism significantly differs from that of acid denaturation, which involves protonation of specific residues (His, Asp, Glu) that may be localized within the protein.[33,34]

This disruption of tertiary interactions indirectly affects secondary structure. In the absence of stabilizing tertiary interactions, helices adopt conformations that are highly dependent on their innate helical propensities.[35] Therefore investigation of the helical propensities of those peptide segments that correspond to helices in the native protein becomes particularly relevant for understanding the character of a cold-denatured ensemble.

An analogue of the A-helix from *pc*-apoMb has recently been studied by Dyson and co-workers.[36] As indicated in Figure 2, the A-helix segment of *pc*-apoMb shares only 72% of its amino acid residues with the corresponding segment in the horse molecule. In addition, every mutation stabilizes helix formation in *pc*-apoMb compared to *eq*-apoMb. When averaged over residues 4−18, mean helical propensities of the A-peptides residues are 1.19 (*pc*-apoMb) vs 1.06 (*eq*-apoMb), significantly favoring helix formation in the sperm whale protein. Three other methods of predicting helical propensity also show that the sperm whale A-helix is significantly more stable than the analogous region in the horse molecule.[37−39]

Work on the sperm whale A-helix was frustrated by that peptide's low solubility in water and the difficulty in incorporating the A-helix region in other relevant segments.[36] Nonetheless CD spectra of the sperm whale A-helix analogue at room temperature do not show typical helix behavior, even upon addition of significant amounts of TFE.[36] As shown in Figure 2, the horse A-peptide would be expected to have even less

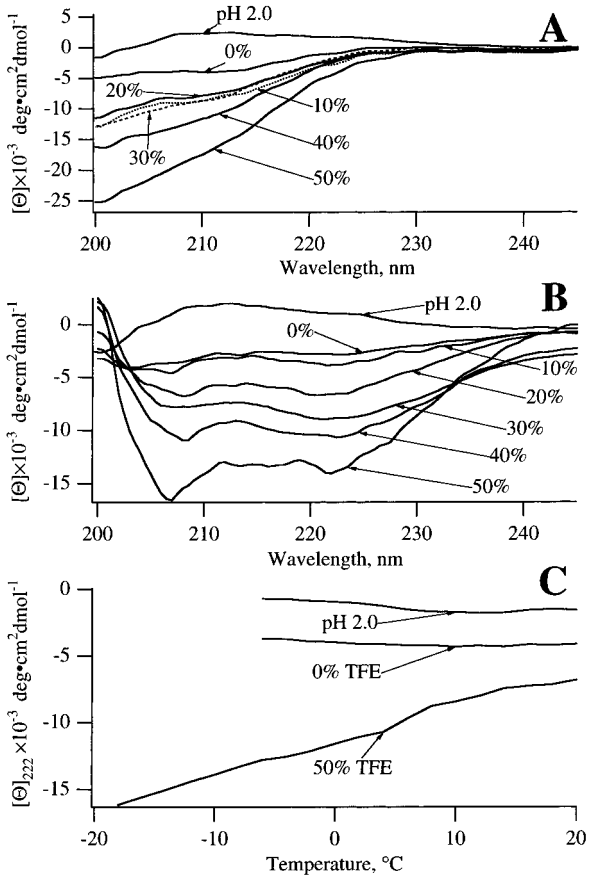

Figure 3. CD data from A-peptide. Samples were 5 μM in peptide and taken under conditions used for far-UV protein measurements. Spectra were smoothed by a Savitzky−Golay algorithm after background subtraction at every set of conditions. (A) A series of spectra taken at different concentrations of TFE at pH 5.9, 23 °C together with that of an aqueous pH 2.0 sample. No helix formation occurs at any TFE concentration. In (B), the experiment was repeated at 0 °C using the same samples as above. In (C) mean ellipticity at 222 nm is plotted as a function of temperature with 2 °C resolution. Spectra shown are for pH 2.0, 0% TFE and for pH 5.9 at 0% and 50% TFE concentrations. A coil-helix transition occurs only in TFE. Mean ellipticity at 222 nm was computed as a weighted average of points between 221 and 223 nm.

helical propensity than the relevant sperm whale region. CD and ^{1}H NMR experiments on the A-peptide reported here show that under conditions favorable for formation of some structure in the G- and H-helices, the A-peptide of *eq*-apoMb does not adopt significant helical structure.

Aqueous *equine* A-peptide has a random-coil CD spectrum at 17 °C, pH 2.0, and 17 °C, pH 5.9 (Figure 3A). Random-coil spectra have been reported to vary from slightly positive with a maximum between 208 and 222 nm to slightly negative with positive slope between 208 and 222 nm.[40] In contrast, helix spectra are always negative, with a pronounced 208/222-nm double minimum for larger helices and a minimum at 222 nm with a negative slope between 208 and 222 nm for very short helices.[41] Neither of these characteristics appear at any of the pH values and TFE concentrations for the room-temperature spectra shown in Figure 3A, indicating that under all of these conditions, the A-peptide does not adopt significant helical populations.

A similar experiment at 0 °C (Figure 3B) does show increasing helix population as the TFE concentration is raised (≈40% in 50% TFE; population estimated using eq 1, discussed in detail below). This increase in helix content at low

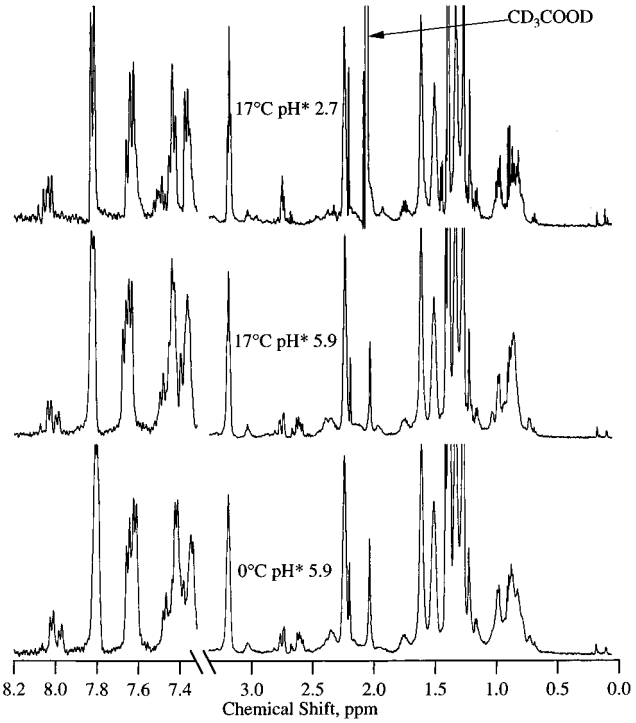

Figure 4. NMR spectra under various conditions for the A-peptide in 60% TFE/D_2O are shown. All FIDs were apodized with a 1-Hz line broadening and then smoothed using a Savitzky−Golay algorithm after Fourier transformation. The top spectrum was taken using an acetate buffer at pH* 2.7, while the bottom two were taken in a phosphate buffer at pH* 5.9. Chemical shift positions come from other A-peptide spectra that had been referenced to TSP.

temperatures is a generally observed phenomenon, both in monomeric peptides[42−44] and native (i.e., above cold-denaturation temperature) proteins (e.g., Figure 6A). However, the A-peptide signal in TFE-free aqueous buffer has no helix signature even at 0 °C.

Mean ellipticity at 222 nm was followed as a function of temperature for the pH 2.0, 0% TFE, pH 5.9, 0% TFE, and pH 5.9, 50% TFE cases (Figure 3C). Offering a measure of circular dichroic baseline, the pH 2.0 mean ellipticity does not significantly change with temperature down to −8 °C. The 0% TFE case is simply a shifted baseline curve, indicating that in the absence of further stabilization the population of helical A-peptide does not increase with decreasing temperature. This is in contrast to the behavior of the TFE-stabilized case where the mean ellipticity at 222 nm decreases throughout the temperature range measured. There is no sharp cooperative transition characteristic of a two-state process as seen for the entire protein (Figure 6). This is not surprising since helical peptide folding is not generally a two-state process.[45]

1D ^{1}H NMR measurements corroborate the CD analysis (Figure 4). They were performed on a Varian Unity Inova narrow bore spectrometer at a field of 500 MHz using residual water presaturation. A-peptide conformation as a function of temperature was investigated in 60% TFE between 0 and 17 °C, at pH* 5.9 and pH* 2.7. Samples were 50 μM in peptide and buffered with 40 mM phosphate (pH* $\geq$ 4.0) or acetate (pH* < 4.0). Temperature readings were verified using the standard neat methanol procedure.

Little chemical shift dispersion and sharp peaks in 60% TFE, both indicative of a random coil, are seen at $T = 17$ °C in the pH 2.7−5.9 range (Figure 4). Particularly notable is the shape of the upfield peaks in the pH* 5.9, 17 °C spectrum. Compared

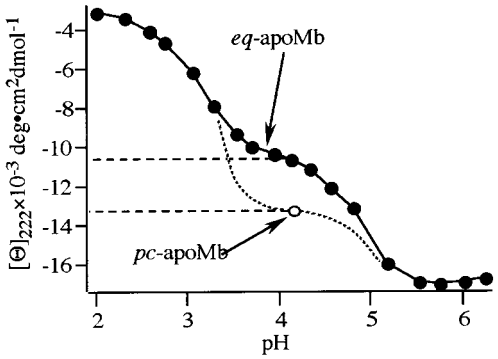

Figure 5. pH dependence of $[\Theta]_{222}$ for *eq*-apoMb, pH 5.9, 22 °C. The *pc*-apoMb acid intermediate data at the transition midpoint (pH 4.2) is also shown for comparison, indicating the low helix content of the *eq*-apoMb I-state.

to A-helix peaks of the native protein (Figure 11, below), the aliphatic region does not show a trailing into the upfield direction. Only upon temperature decrease to 0 °C does the aliphatic envelope trail further upfield, indicating that some of the interactions which cause a negative secondary chemical shift in the native protein are beginning to be sampled. A 0−60% TFE titration at 17 °C on the A-peptide solution using deuterated TFE at 10 μM concentration showed negligible changes in the spectra (data not shown).

The G- and H-helices show a higher helix-forming propensity than that observed for A-peptide. H-helix peptide and an E109Q analogue of the G-helix from *pc*-apoMb have been synthesized and thoroughly characterized in aqueous and TFE buffers by Dyson and co-workers.[43,46,47] Unlike the <75% homology of the A-peptides, G- and H-helix segments have respectively 90 and 93% homology between horse and sperm whale proteins (Figure 2). Due to the high homology and insignificant difference in G- and H-helical propensities, the *pc*-apoMb peptides are directly relevant to the discussion of the *equine* protein. Isolated H-helix analogue has significant helical structure (≈35%) in TFE-free water at 0 °C.[43] The G-helix analogue does not show significant helical structure in water but readily adopts helical structure at room temperature upon addition of TFE (68% in 15% TFE, room temperature).[47] Under neither of these conditions does *eq*-A-peptide offer evidence for helical structure in our NMR or CD measurements. These results are qualitatively predicted by simple mean helical propensity calculations for the three horse protein helices (Figure 2). The H-helix with 1.20 far exceeds the G-helix's 1.09, which marginally exceeds the A-helix's 1.06. For sperm whale, the corresponding three numbers are 1.22, 1.12, and 1.19, showing a dramatic increase in the A-helix stability of that protein.

In summary, although the A-peptide sequence forms a stable helix in *eq*-apoMb, in isolation it is the least stable of the three helices involved in AGH-packing. The *eq*-A-peptide does not adopt any helical structure in room- or even low-temperature aqueous solution and has a lower helix propensity than does *pc*-A-peptide.

3. CD Spectroscopy. CD measurements were performed on a Jasco J-720 spectropolarimeter using a circulating bath and jacketed aluminum cell holder for temperature control. The temperature was varied at a maximum rate of 1 °C/min and monitored by a thermocouple attached adjacent to the sample cell. All CD samples were prepared in 40 mM phosphate buffers. Far-UV CD measurements were made in 0.3 mm cells at concentrations from 30 to 50 μM, while near-UV measurements were taken in a standard 1-cm cell at approximately 100 μM. The spectropolarimeter was calibrated using ammonium camphorsulfonate-*d*-10 at 290.5 nm.[48]

Accurate determination of the mean residue ellipticity for a given protein sample is dependent on a number of factors including the purity of the protein sample, determination of protein concentration, and proper calibration of the instrument. In the past, differences in purification protocols, methods of concentration determination, and instrument calibrations have resulted in deviations of up to 15% in the mean residue ellipticities published by various research groups for the same protein, thereby making comparisons difficult.[13,41,49] All CD data presented here were measured using a single calibrated spectropolarimeter, and all protein concentrations were consistently determined as detailed above, thereby allowing for more meaningful comparisons among our data.

Protein far-UV spectra generally can be represented as linear combinations of model spectra for α-helix, β-sheet, β-turn, and random coils.[41] Several different variations of this general multicomponent analysis have been developed to predict protein secondary structure from CD data. These methods differ primarily in the choice of reference spectra and calibration via X-ray data. Although the accurate prediction of β-sheets and turns has proven difficult and highly method-dependent, the determination of α-helix content has shown excellent agreement with X-ray data and has proven to be consistent regardless of the method chosen.[50] All CD-based α-helix fractions reported here were calculated using

$$[\Theta]_{222} = -31\,900 f_h - 200 \qquad (1)$$

where f_h is the helical fraction of the protein of interest. This simplified equation was determined specifically for apoMb as the pure helix signal was derived using an experimentally determined CD signal of −25 700 deg cm^2 dmol^{-1} for *eq*-Mb and a helical content of 80% based on X-ray data. Similarly, the CD value of *eq*-apoMb in 6M GuHCl, pH 2.0 was used for the random-coil contribution. The equation neglects β-sheets since none are present in folded myoglobin and β-turns since they contribute <2% of the signal at 222 nm.[48,51] Compared to equations reported in the literature,[41] eq 1 is conservative in the sense that it predicts relatively high helix fractions and probably underestimates the amount of cold denaturation.

Figure 5 shows the mean residue ellipticity at 222 nm, 22 °C as a function of pH for *eq*-apoMb and *pc*-apoMb. The results are in good agreement with previous work.[19,49] *eq*- and *pc*-proteins are fully folded near pH 6.0, while the I-state is 41% helical for *pc*-apoMb and only 35% helical for *eq*-apoMb. On the basis of the *eq*-Mb X-ray structure, fully intact A-, G-, and H-helices correspond to 40%. Together with NMR data,[20] this indicates that although the *pc*-I-state likely has an intact AGH-core, this cannot be the case for the significantly less structured *eq*-I-state. According to the X-ray structure, fully intact G- and H-helices correspond to 30% helicity. This fact combined with the known greater helical propensity of the G- and H-helices would indicate that the *eq*-I-state has at least a partially unfolded A-helix.

Temperature-dependent CD curves for *eq*-apoMb at pH 4.1 and pH 5.9 are shown in Figure 6A. Each curve combines repeated experiments covering overlapping temperature regions and were reproducible with different samples. The estimated uncertainty of the combined data is ±500 deg cm^2 dmol^{-1}. The solid line is a fit to a thermodynamic three-state model with

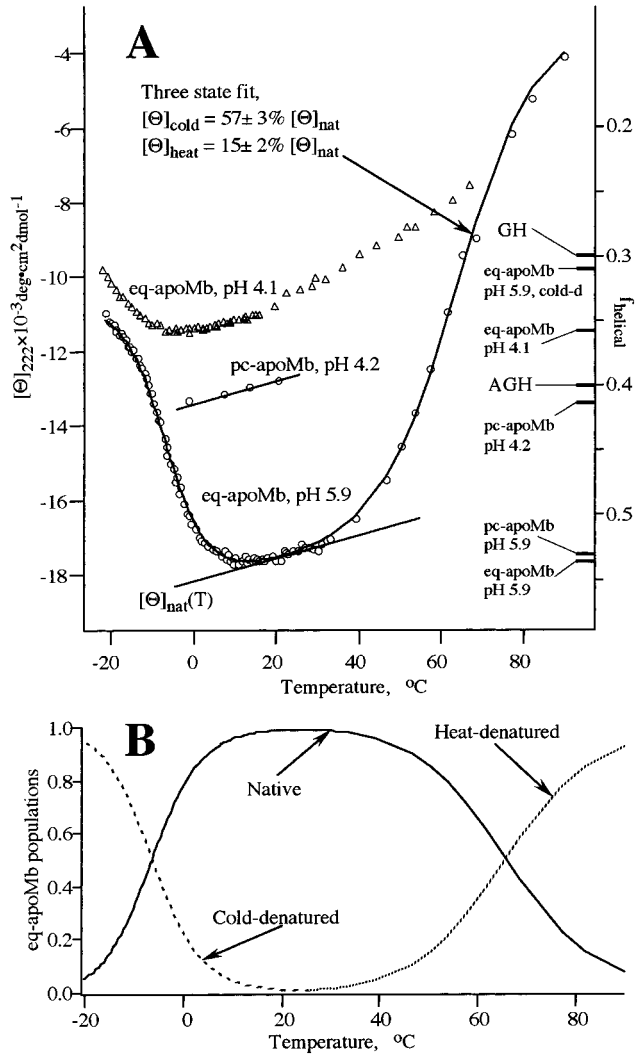

Figure 6. (A) Temperature dependence of $[\Theta]_{222}$ for 40 mM phosphate pH 5.9, 4.1 *eq*-apoMb, and pH 4.2 *pc*-apo Mb for comparison. Native *pc*-apoMb at room temperature had a CD similar to that of *eq*-apoMb but shows only half the amount of cold denaturation at −8 °C (data not shown). Fraction helical, $f_{helical}$, is plotted on the right axis with various important reference points provided. Protein fractions were calculated using eq 1, and the intact AGH- and GH-helical reference points were determined from X-ray data.[51] A thermodynamic three-state fit of the pH 5.9 *eq*-apoMb data was performed using eqs 2−6 and is represented by the solid curve. An accurate fit required a slightly temperature-dependent native-state helix content as indicated by the solid line $[\Theta]_{nat}(T)$, which shows increased helix stability at lower temperatures. (B) Temperature dependence of the cold-denatured, heat-denatured, and native-state populations obtained from the fit in (A).

$$\Delta G_{NH} = \Delta G^{(o)}_{NH} - (T - T^{(o)}_{NH})\Delta S^{(o)}_{NH}$$
$$\Delta G_{NC} = \Delta G^{(o)}_{NC} - (T - T^{(o)}_{NC})\Delta S^{(o)}_{NC} \quad (2)$$

$$K_{NH} = e^{-\Delta G_{NH}/RT} \qquad K_{NC} = e^{-\Delta G_{NC}/RT} \quad (3)$$

$$f_N = 1/(K_{NH} + K_{NC} + 1) \quad (4)$$

$$f_H = K_{NH}/(K_{NH} + K_{NC} + 1) \quad (5)$$

$$f_C = K_{NC}/(K_{NH} + K_{NC} + 1) \quad (6)$$

where f_N, f_H and f_C represent the native/heat-denatured/cold-denatured fractions and K_{NH} and K_{NC} represent the corresponding equilibrium constants. A slightly temperature-dependent native-state helicity was required for an accurate fit and is represented by the solid line $[\Theta]_{nat}(T)$, which indicates increased helix content at lower temperature for the native state. A plot of the native, heat-denatured, and cold-denatured state populations is shown in Figure 6B and shows no significant overlap of cold- and heat-denatured populations. Both cold and heat denaturation are well fitted by cooperative two-state transitions.

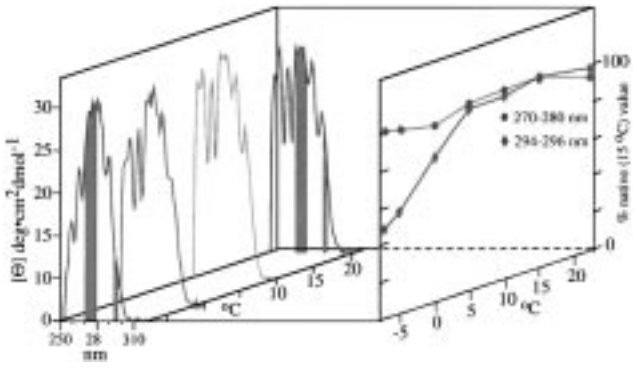

Figure 7. Near-UV CD spectra of *eq*-apoMb as a function of temperature. The blue and red bands mark the 270−280-nm and 294−296-nm regions, respectively; their percentage of native values vs temperature are plotted on the right panel. All percentages were calculated using the 15 °C value as native.

The fit indicates that the cold-denatured state corresponds to only 31% helical structure, significantly less than the I-state. The I-state itself cold denatures (Figure 6) and is clearly not the target of cold denaturation from the native state. Furthermore, the A-, G-, and H-helices, which comprise the hydrophobic core, can no longer all be intact in the cold-denatured state since its 31% helical structure is well below the 40% required for fully folded A-, G-, and H-helices based on the X-ray structure. This is in contrast to the I-state of *pc*-apoMb (Figure 6), which shows about the same helical content as intact A-, G-, and H-helices. A fairly stable AGH-core in *pc*-apoMb is indicated by NMR studies,[20] and kinetic studies show that the BCDEF-helices are more sensitive to denaturation by hydrophobic additives (urea) than the AGH-core.[23]

Near-UV CD and fluorescence (discussed below) provide evidence that the residual far-UV signal is mostly associated with remaining GH-structure, while the AGH-core dissolves. Near-UV CD in the 250−310 nm region has long been used as a measure of protein tertiary structure, or more precisely the rigidity of the environment around aromatic side chains.[52] Figure 7 shows a 20 °C spectrum in good agreement with previous work.[13] Raw data for three other temperatures along with a temperature-dependent average of both the 270−280 and 294−296-nm ranges are shown as well.

Near-UV CD is not as well understood as far-UV CD since spectra in the aromatic region from 250 to 310 nm are composed of a combination of environmentally sensitive phenylalanine, tyrosine, and tryptophan signals. Loss of side chain rigidity results in decreased CD signals (essentially zero for random peptides). Loss of tertiary structure also results in smoother spectral structure throughout the 250−310-nm region.[52] As in the case of absorption spectra, the region to the red of 290 nm is due to tryptophan side chains only,[53] while the 270−280-nm region contains significant contributions from tyrosine also. Due to the small absorption cross section of phenylalanine at wavelengths greater than 270 nm, tyrosine and tryptophan dominate that region.

It is evident from the spectra shown in Figure 7 that significant cold denaturation is occurring, indicated by the decrease in intensity and loss of spectral structure at −7 °C as compared to at 20 °C. The 295-nm tryptophan region[53] shows

a decrease in intensity to less than 50% of the native value with no leveling-off at the lowest temperature of −7 °C currently possible in the required 1-cm cell. This indicates a loss of rigid structure on the hydrophobic side of the A-helix and disruption of the AGH-hydrophobic core. The 250−260-nm signal, where the tryptophan absorption cross section again dominates, also shows a decrease in intensity and structure.

The 270−280-nm signal, where tyrosine makes its largest contribution, remains essentially unchanged. This is consistent with an intact GH-complex since both *eq*-apoMb tyrosines and three of the phenylalanines are located within the G- and H-helices. From NMR data[17] it is known that the C-helix is destabilized upon heme removal, even in native apoMb, so the 270−280-nm signal probably contains less contribution from tyrosine 103 (Y103). However, the more congested nature of near-UV CD spectra below 290 nm precludes any precise estimate of the remaining structure in GH. It should be noted that no significant loss of side chain rigidity is observed over the entire spectral range up to at least 35 °C, where aggregation and precipitation precludes further spectroscopy at the required sample concentrations.

In summary, the far-UV CD data indicate a two-state transition of *eq*-apoMb beginning at 3 °C. The resulting cold-denatured state has A-helix content comparable to only the GH-helices and clearly less than the full AGH hydrophobic core seen in the *pc*-apoMb I-state. The near-UV CD data show disruption of the rigid hydrophobic core sampled by the W7 and W14 side chains in the A-helix and also indicate retention of some rigidity in the GH-helices.

4. Fluorescence Spectroscopy. The fluorescence maximum of buried tryptophan residues occurs near 330 nm as compared to fully solvated tryptophan fluorescence, which is red-shifted to near 350 nm. Since the fluorescence of *eq*-apoMb is dominated by the two tryptophans in the A-helix, denaturation of the AGH-hydrophobic core should result in the solvation of these two tryptophans and thus may be monitored by the red-shifting of the fluorescence maximum. Furthermore, relative fluorescence intensities can also provide some insight into protein conformation, especially when the fluorescence is dominated by one or two fluorophores. It has been observed by both acid and GuHCl denaturation that complete denaturation of the AGH-core is preceded by a hyperfluorescence maximum.[35,54−57]

All fluorescence measurements were performed on an ISS photon-counting fluorometer with 280-nm excitation, using temperature control as in the CD measurements. The temperature was varied at a maximum rate of 2 °C/min as monitored by a precalibrated thermocouple attached next to the sample cell. All samples were prepared in 40 mM phosphate buffer unless otherwise noted. Some measurements were also performed with excitation at 295 nm, yielding similar results (data not shown).

Figure 8 provides a detailed summary of the cold denaturation of *eq*-apoMb as monitored by fluorescence. Raw spectra for pH 5.9 *eq*-apoMb at various temperatures are shown in panel A. As the temperature is decreased, the absolute fluorescence intensity maximum red-shifts starting at 3 °C due to the appearance of a distinct fluorescence shoulder centered at 350 nm. The shoulder is due to the presence of solvated tryptophan side chains, which appear as the equilibrium shifts toward an apparently solvent exposed, cold-denatured state upon cooling below 3 °C.

To clarify this point, the set of 11 spectra was analyzed in two different ways. First, spectra were fitted to a linear combination of two basis spectra: the 20 °C native-state apomyoglobin spectrum and an experimentally determined 6M GuHCl spectrum representing the denatured state. The resulting fit for the −15 °C spectrum is shown on the back panel of Figure 8A, together with the "denatured" intensity component. The high quality of the fit indicates that the choice of basis function is reasonable and verifies the presence of solvated tryptophans. The fraction of the native basis state amplitude vs temperature is shown in panel B and clearly indicates the onset of cold denaturation below 3 °C.

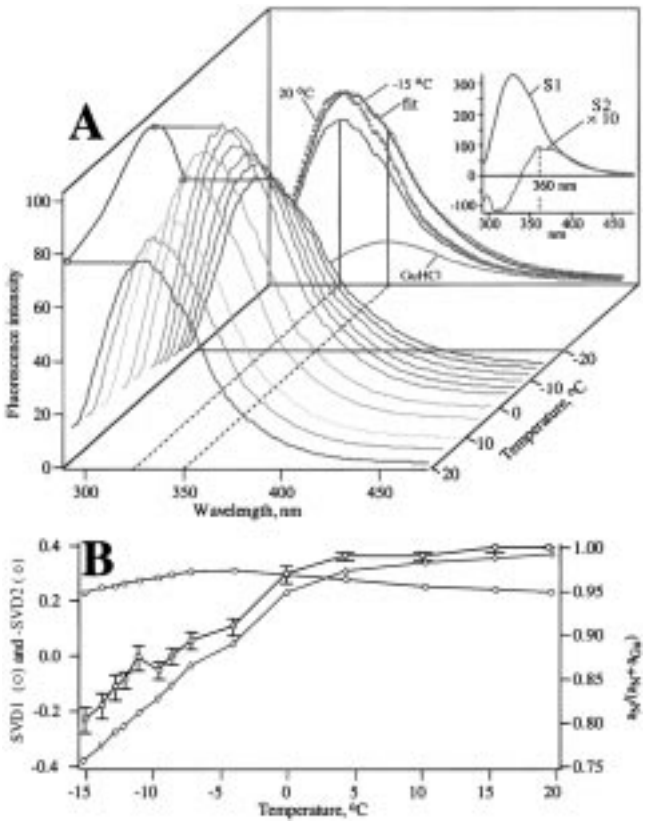

Figure 8. (A) Fluorescence spectra of *eq*-apoMb in pH 5.9, 40 mM phosphate at a series of temperatures from 20 to −15 °C. Spectra were three-point box smoothed, and the peak intensities as a function of temperature are shown on the left panel, indicating hyperfluorescence before a decrease in fluorescence upon cold denaturation. Spectra were fit to a linear combination of the native state apomyoglobin spectrum at 20 °C and an experimentally determined 6 M GuHCl-denatured spectrum. The fitted −15 °C spectrum with a 350-nm shoulder and the native spectrum are shown for comparison on the back panel of (A). The corresponding native and denatured components are also shown as solid red and blue lines, respectively, and the native component fraction versus temperature is plotted in black in (B). The data were also analyzed using SVD, resulting in two significant components required for data reconstruction, which are shown in the inset of (A) and labeled S1 and S2. The coefficients of S1 and −S2 are plotted versus temperature in (B). S1 tracks the hyperfluorescence, while S2 tracks the onset of the shoulder at 350 nm due to cold denaturation.

The 11 spectra were also analyzed using singular value decomposition (SVD).[58] This resulted in only two significant components (S1 and S2) required for accurate data reconstruction at all temperatures, indicative of a two-state process. They are shown on the back panel. The primary component S1 represents an average spectrum, while S2 accounts for the growth of the 350-nm shoulder and loss of intensity at 328 nm. The weighting coefficients of S1 and S2 are also plotted vs temperature in panel B. The S2 coefficient tracks the two-state spectral fit, marking the onset of cold denaturation at roughly

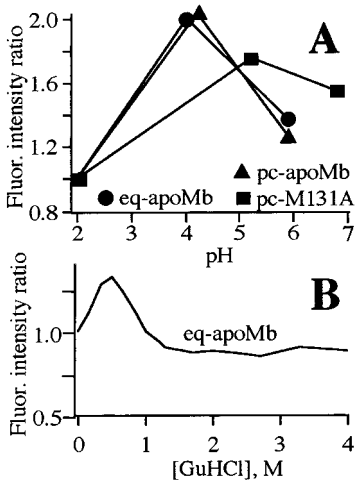

Figure 9. (A) pH denaturation as monitored by peak fluorescence intensity is plotted for *eq*-apoMb, *pc*-apoMb, and *pc*-M131A mutant. Data are presented as a ratio to its respective pH 2.0 state. While the wild-type molecules show similar hyperfluorescence, the M131A mutant shows more fluorescence in the native state and less hyperfluorescence. (B) Peak fluorescence intensity versus GuHCl concentration for *eq*-apoMb, showing hyperfluorescence before full denaturation. Data has been scaled to 1 for the 0 M sample.

3 °C. Unlike the previous analysis, SVD is model independent. The fact that different fluorescence analyses yielded the same result using two fitting functions provides strong evidence for a two-state unfolding process.

However, apoMb peak fluorescence shows a pronounced local maximum at −5 °C (left panel of Figure 8A). While S2 traces the onset of the 350-nm shoulder at 3 °C, S1 traces the average fluorescence intensity and shows this hyperfluorescence maximum at −5 °C (Figure 8B). Such a local maximum is also observed upon pH and GuHCl denaturation of *eq*-apoMb (Figure 9) and *pc*-apoMb.[54−57] The effect is accentuated because tryptophan fluorescence intrinsically increases at lower temperature (both for the monomer and in the unfolded A-peptide, data not shown), but even scaling by a tryptophan reference does not remove the hyperfluorescence maximum completely. Rather, it results in a less pronounced maximum at higher temperature.

The fact that hyperfluorescence is already underway before appearance of the 350-nm shoulder indicates that the hyperfluorescent AGH-core is initially structurally similar to the native state. Since the hyperfluorescence is not in concert with the spectral shift and CD data, it would appear to be associated with a "pre-transition" loosening of the apoMb structure, which does not completely disrupt the hydrophobic AGH-core. This is then followed by disruption of the AGH-core and solvent exposure of the tryptophan residues at lower temperatures. In contrast, during acid denaturation the hyperfluorescence tracks other measures of unfolding in both *equine* (Figures 5 and 9) and sperm whale proteins,[22] and can be assigned to a bona fide intermediate, the I-state.

The M131−W14 interaction plays an important role in these fluorescence properties. Methionine is a Dexter quencher of tryptophan fluorescence,[59,60] and the two residues are in dipolar contact in the native state of *eq*-apoMb.[15] Figure 9A shows the pH-dependent fluorescence of native *eq*-apoMb, *pc*-apoMb, and M131A *pc*-apoMb. The M131A native and I-state points are shown at higher pH because the lower stability of the mutant shifts the pH titration curve. The peak fluorescence intensity of the native M131A mutant (pH 6.8) is significantly higher that of native *eq*- and *pc*-apoMb. Furthermore, strong hyperfluorescence occurs for both native *eq*-apoMb and *pc*-apoMb, whereas the M131A mutant shows only slight hyperfluorescence. This observation provides strong evidence both that M131 indeed quenches W14 fluorescence in the fully folded state and that the hyperfluorescence is associated with a slight loosening of the hydrophobic core, resulting in solvent exposure of the A-helix tryptophans. Finally, as shown in Figures 8A and 9, cooling below −5 °C as well as pH and GuHCl denaturation ultimately result in a steady decrease in peak intensity and loss of the A−(GH)-hydrophobic core.

In summary, the temperature dependence of *eq*-apoMb fluorescence indicates a two-state transition beginning at 3 °C toward a cold-denatured state with a dissolved AGH-core, which exposes the tryptophan residues in the A-helix to the solvent. The early stages of this transition are accompanied by hyperfluorescence with a different temperature dependence, which may be due to a "pre-transition" loosening of the AGH-core as sampled by the M131−W14 interaction.

5. Infrared Spectroscopy. The amide I′ band, located between 1600 and 1700 cm^{-1}, corresponds to the carboxyl stretching mode of the deuterated backbone and Asn and Gln side chain amide units. Particularly sensitive to the effects of hydrogen bonding, this band has frequently been employed as an indicator of protein secondary, and even tertiary, structure.[61] Upon helix melting the previously intraprotein hydrogen-bonded amides will be solvent exposed, leading to a change in the resonance frequency of the peptide unit, particularly the C═O stretch. Here we probe the amide I′ band of *eq*-apoMb as a function of temperature for various pH* values.

Temperature-dependent infrared measurements of the amide I′ band in D_2O were performed on a Nicolet Magna-IR 760 spectrometer, using a 125 μm Mylar-spacer between two CaF_2 windows, a setup consistently allowing access to temperatures of −10 °C before freezing. Samples were between 100 and 300 μM in protein, with 40 mM phosphate buffering. Temperature calibration was performed by placing a thermocouple directly into an organic solution between the CaF_2 windows.

The amide I′ band has an intrinsic small temperature dependence, as shown by a barely resolvable red-shift of denatured protein absorbance between 12 and −10 °C (pH*'s 3.0 and 13.5, data not shown). On the other hand, the spectra shown in Figure 10 at pH* 5.9 show peak broadening and a clear red-shift of the absorbance maximum with decreasing temperature. Indeed, the spectrum at −10 °C, pH* 5.9 closely resembles the spectrum at pH* 3.0 and −10 °C, motivating modeling the temperature-dependent data at pH* 5.9 as a linear combination of the pH* 5.9, 12 °C "native spectrum" and the pH* 3.0, −10 °C "denatured" results. The shape of the resultant curve $\chi_C(T) = f_C/(f_N + f_C)$ shows a transition beginning near 3 °C (Figure 10B). The temperature-dependent data have also been decomposed using SVD.[58] S1 reflects the temperature-averaged data, and only S2 shows a significant systematic temperature dependence, plotted in Figure 10B. SVD modeling shows the same transition beginning near 3 °C and closely follows the shape of χ_C, indicative of a concerted two-state process.

Previously, results have indicated that the amide I′ band of *eq*-apoMb undergoes a blue-shift upon *heat* denaturation, which also exceeds the intrinsic temperature shift.[62] Because of the difficulty of predicting vibrational frequencies of a particular hydrogen-bonded configuration, [63] we cannot make particular structural arguments to explain a particular shift's direction and magnitude. Our data indicate that intraprotein hydrogen bonds undergo denaturation commencing near 3 °C, eventually leading

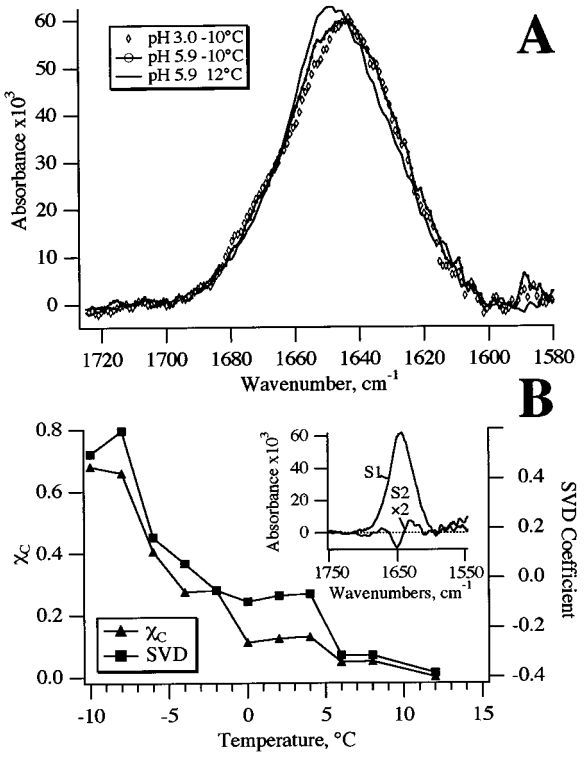

Figure 10. (A) Reconstructed, baseline-subtracted FTIR absorbance spectra of the amide I′ band of *eq*-apomyoglobin at different pH* and temperature combinations. To remove inconsistencies due to imperfect purge conditions, background spectra taken at each temperature and buffer condition were multiplied by a near-unity correction and shifted by a small offset before subtraction. Small water vapor transitions were removed by directly subtracting a measured water vapor spectrum. The cold-denatured spectrum lies closer to the pH* 3.0 denatured spectrum than to the native spectrum. (B) Subtracted spectra as a function of temperature were decomposed using the SVD algorithm, which required two components for the amide I′ peak shape. Higher components containing only noise were discarded, and the data was reconstructed from the four most significant components following Savitzky−Golay smoothing. The inset contains the first- and second-order components. The second-order singular value tracks the shift in line shape upon cold denaturation and is plotted in the bottom panel. Also shown is the unfolded spectral fraction χ_C obtained by modeling the pH* 5.9 data at various temperatures as a linear combination of the native (pH* 5.9, 12 °C) and denatured (pH 3*, −10 °C) data using a least-squares fit.

to a spectrum close to that of the denatured pH* 3.0, −10 °C state. At 1655 and 1630 cm^{-1}, the intensity change (≈10%) is sufficient to serve as a probe of decreasing secondary structure upon cold denaturation.

6. NMR Spectroscopy. The ABGH-interface of *eq*-apoMb has been a target of NMR characterization since the initial 2D investigation in 1990.[15] Since then, a number of different groups have used NMR to verify the existence of the native state's AGH-hydrophobic core in *eq*-apoMb and *pc*-apoMb.[16−18] This work provides many useful chemical shifts and NOE connectivities.

The evolution of specific structural elements during cold denaturation could in principle be followed vis-à-vis the normalized intensity of a relevant proton−proton NOE as the temperature is lowered. In practice, ^{1}H resonances that are well-resolved in the native spectrum disappear upon cold denaturation, often without signs of significant broadening, presumably reappearing at their statistical coil positions in a densely crowded region (see below). Alternatively, isotopically enriched protein has been used to characterize residual structure in cold-denatured barstar, taking advantage of the $d_{N,N(i,i+1)}$ NOEs in the HSQC−

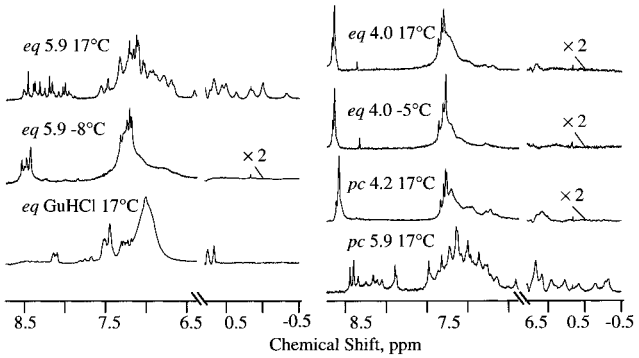

Figure 11. NMR spectra of horse and sperm whale apomyoglobin under various conditions. All were 100% D_2O solutions with data workup as reported in the text. Protein type, pH*, and temperature for each spectrum are indicated on the traces. Several upfield region have been multiplied by two to show small features.

NOESY−HSQC spectrum.[64] It is not clear that this type of experiment would offer any further relevant information when trying to verify the *disappearance* of structure. However, careful consideration of 1D spectra can yield some qualitative and comparative information about particular states of the proteins studied. Here the assignments of Cocco and Lecomte are used to analyze 1D, ^{1}H spectra of *eq*-apoMb and *pc*-apoMb taken at different temperatures and pH*'s.

Spectra were acquired under conditions used for A-peptide at concentrations below 700 μM. To prevent probe damage in case of accidental freezing, standard 4-mm NMR tubes were coated with proton-free Teflon and brought to a total diameter of 5 mm. All resonances were referenced to sodium 3-(trimethylsilyl)-1-propanesulfonate (TSP), or in the case of *pc*-apoMb, to shifts available from the literature.[16] Temperature runs were taken nonspinning, and in each case a room-temperature spectrum was taken after the coldest spectrum in the series. It was always identical in appearance to the spectrum obtained before cold denaturation, showing the reversibility of the process. Apodization was applied in the frequency domain by smoothing downfield regions using a Savitzky−Golay algorithm.

The upfield regions of the spectra required further processing. The large aliphatic peak near 0.90 ppm contains many unresolved methyl and methylene resonances, which in 1D offer no information about cold denaturation. However, several interesting resonances appear as shoulders or small peaks on the upfield tail of this peak between 0.6 and −0.4 ppm. To more clearly see these interesting features, the methyl/methylene envelope was modeled as a linear combination of two positively weighted Lorenztians (both centered downfield of 0.75 ppm) and subtracted from the spectra.

The 1D spectra for the native states of both the *pc*- and *eq*-apoMb in Figure 11 show large chemical shift dispersion and narrow lines. Shifts may be seen as far upfield as −0.38 ppm (V17 $C^{\gamma 1}H_3$) in both proteins. Many of the peaks in the aromatic and upfield regions can be assigned to specific residues on the basis of previous 2D work (Table 1).[15] The local environment of these residues is affected by ring currents (e.g., Trp 14 and His 24 effect on Val 17 $C^{\gamma 1}H_3$ protons) and many other interactions that induce secondary chemical shifts. Upon disruption of local structure these well-resolved resonances will either disappear (and reappear at a denatured chemical shift value) or become broadened due to conformational fluctuations on the NMR time scale. The spectral changes observed are of a different character for different denaturation methods. The analysis employed to assess this character does not resolve

TABLE 1: Clearly Assignable Peaks in the 1D NMR Spectrum of *Eq*-apoMb at 17 °C

resonance	ppm	position	behavior
V17 $C^{\gamma 1}H_3$	−0.38	A-helix	loses intensity/disappears
L2 $C^{\gamma 2}H_3$	−0.05	amino end	loses intensity/disappears
V17 $C^{\delta 2}H_3$	0.10	A-helix	loses intensity/disappears
L2 $C^{\delta 1}H_3$	0.13	amino end	loses intensity/disappears
L40 $C^{\delta 2}H_3$	0.35	C-helix	loses intensity/disappears
L2 $C^{\delta 1}H_3$	0.13	amino end	loses intensity/disappears
L40 $C^{\delta 1}H_3$	0.37	C-helix	loses intensity/disappears
L115 $C^{\delta 1}H_3$	0.49	G-helix	loses intensity/disappears
L115 $C^{\delta 2}H_3$	0.61	G-helix	loses intensity/disappears
L49 $C^{\delta 2}H_3$	0.70	CD-coil	loses intensity/disappears
F46 $C^{\alpha}H$	5.01	CD-coil	no change
F33 $C^{\zeta}H$	6.19	B-helix	shifts/broadens
H24 $C^{\delta}H$	6.36	C-helix	broadens/disappears
F43 $C^{\zeta}H$	6.49	CD-coil	loses intensity/disappears
F33 $C^{\epsilon}H$	6.72	B-helix	broadens
F106 $C^{\delta}H$	6.75	G-helix	broadens
F46 $C^{\delta}H$	6.87	CD-coil	broadens
F106 $C^{\delta}H$ or H119 $C^{\delta}H$	6.90	G-helix	broadens
	6.90	G-helix	

[a] Behavior is upon cold denaturation to −8 °C. Chemical shifts are from Cocco and Lecomte.[15]

structural issues down to single residues. However, it does yield comparative information for the several states of *pc*- and *eq*-apoMb as well as indicates the nature of the cold-denaturation transition.

Readily apparent from Figure 11 is the complete absence of well-resolved upfield resonances for cold denatured *eq*-apoMb. The upfield region of this spectrum lacks resonances that are present even in the 6 M GuHCl-denatured spectrum. At the same time the well-dispersed downfield resonances collapse into two narrower features centered at 8.4 and 7.2 ppm. This latter feature gives evidence of fluctuating structure on the order of the NMR time scale (Kilohertz), in that its upfield tail (7.2−6.5 ppm) shows broadened peaks that can be traced continuously to the native state as a function of temperature (Table 1).[65]

The *pc*-apoMb and *eq*-apoMb I-state spectra (taken at their pH*'s of maximal stability at 17 °C, Figure 5) do not show this type of behavior. Both contain features conspicuously absent from the corresponding pH* 5.9 cold-denatured spectra. This residual structure, centered at 0.65 ppm for *eq*-apoMb and 0.55 ppm for *pc*-apoMb, also disappears when the I-state is cold-denatured (Figure 11). In a previously published spectrum of the *pc*-apoMb I-state[19] the unsubtracted methyl/methylene envelope camouflaged these features. The downfield regions show less peak broadening in the I-state at 17 °C than in the cold-denatured pH 5.9* state. For *pc*-apoMb in particular, the I-state region from 7.2 to 6.5 ppm contains more resolvable resonances with narrower line widths than either the cold- or GuHCl-denatured states.

In *pc*-apoMb the I-state AGH-complex retains much residual structure that involves specific, nativelike tertiary interactions at pH* 4.2.[20,22] A smaller amount of residual structure (still exceeding the GH-helix fraction, Figure 6) exists as well in the *eq*-apoMb I-state. That it is less than for *pc*-apoMb is evidenced by both the smaller CD signal and the smaller dispersion and broader peaks both up- and downfield in the I-state *eq*-apoMb NMR spectrum. However, the mere fact that the *eq*-apoMb acid intermediate can be cold-denatured (CD Figure 6 and *eq*-pH 4.0*, −5 °C spectrum in Figure 11) indicates that it is probably stabilized by a residual hydrophobic core. The spectrum of cold-denatured *eq*-apoMb at −5 °C in Figure 11 was not taken at a temperature cold enough to fully remove all residual structure from the acid-intermediate state. It is clear,

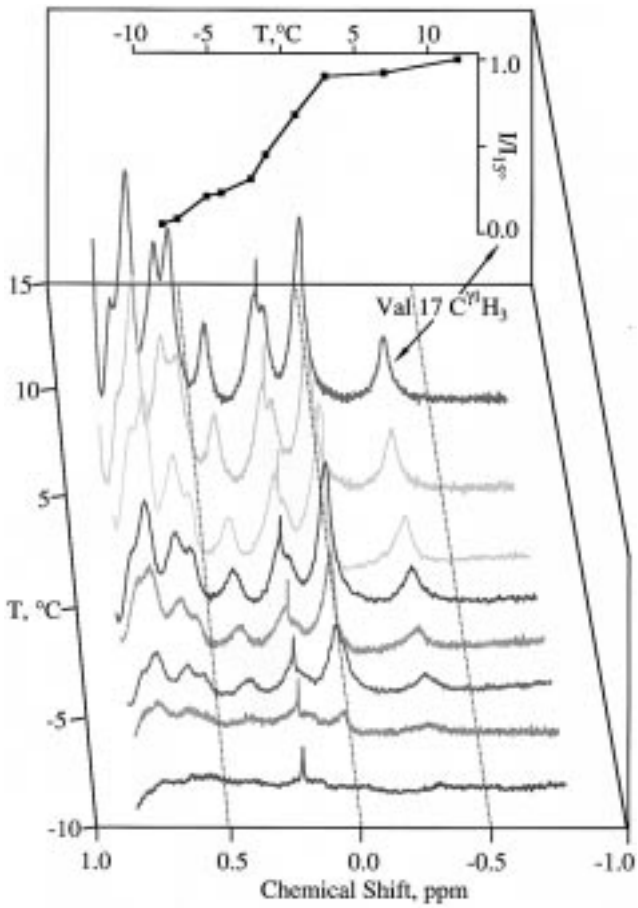

Figure 12. Upfield region of 700 μM *eq*-apoMb pH 5.9 as a function of temperature, with subtracted methyl/methylene envelope (see text). The back panel shows the intensity of the Val 17 $C^{\gamma 1}$ H_3 peak as a function of temperature. It was normalized to the intensity of the TSP standard at every temperature that could be reliably determined due to its relative narrowness. Peak assignments from Cocco and Lecomte are summarized in Table 1.

however, that cooling removes or collapses spectral features during cold denaturation of the I-state of *eq*-apoMb, presumably by disruption of the residual tertiary structure.

The idea that the *eq*-I-state is less structured than the *pc*-I-state preceding its cold denaturation is also supported by NMR spectroscopy at higher pH. At pH* 4.8,[66] the *eq*-apoMb spectrum looks very similar to the relatively featureless pH* 4.0 spectrum reported here, while the *pc*-apoMb spectrum contains more resonances with large secondary chemical shifts compared to the pH* 4.2 spectrum shown here. These data specifically shows that side chain resonances of L2, V17, L40, and L76 are all still readily discernible upfield of 0.6 ppm in the *pc*-apoMb I-state. The spectra clearly show the higher lability to pH titration of *eq*-apoMb structure relative to that of *pc*-apoMb.

Unlike the three-state acid-denaturation process, consideration of the upfield region during pH* 5.9 cold denaturation of *eq*-apoMb indicates a concerted two- state transition beginning near 3 °C (Figure 12). All upfield peaks show a simultaneous decrease in intensity without noticeable broadening. Notably, upfield resonances in as different positions as L2 $C^{\delta 2}H_3$ (amino terminal random coil, seen at −0.05), V17 $C^{\gamma 1}H_3$ (A-helix), L40 $C^{\delta 2}H_3$ (C-helix, seen at 0.35 ppm), and L115 $C^{\delta 1}H_3$ (G-helix, seen at 0.49 ppm) all disappear following a similar pattern.

In summary, NMR ranks protein states by structure content based on spectral appearance. Cold-denatured *eq*-apoMb has

less structure than acid-intermediate *eq*-apoMb, which in turn has less structure than acid-intermediate *pc*-apoMb, which in turn has less structure than native *pc*- or *eq*-apoMb: results mirroring those obtained by CD. Peak intensities indicate that the local A to GH-interactions of *eq*-apoMb are disrupted upon cold denaturation at L2, V17, and presumably intermediate positions.

Discussion

In temperature-jump experiments initiated from the cold-denatured state of *eq*-apoMb, two phases have been observed: a submicrosecond one resulting in decreased quenching of tryptophan residues and a few microseconds one resulting in increased quenching of tryptophan residues.[8] No further significant phases are observed up to ≈1 ms. A better understanding of the structural features specific to the initial cold-denatured ensemble translates directly into stronger constraints on the structural changes associated with the fast refolding phases of apoMb.

Significant differences between the heat- and cold-denatured states of a particular protein are not always observed,[5] but it should be clear from the previous section that there are important structural differences between the acid-, heat-, and cold-denatured states of apoMb. At low pH, protein side chains (particularly His, Glu, and Asp) become protonated, leading to disruption of local structure.[33,34] Heat denaturation proceeds because at high temperatures an enormous number of states with high configurational entropy become accessible. Cold denaturation occurs primarily because of the decreased entropic cost of solvating hydrophobic side chains at low temperature.[12,67]

Specifically, decreasing the temperature of a pH 5.9 solution of *eq*-apoMb causes a concerted disruption of the AGH-hydrophobic core below 3 °C, as the inner face of the A-helix becomes solvent-exposed. Upon transition, the GH- complex appears to retain at least some nativelike structure, while the A-helix probably melts due to its low helix propensity in isolation.

The firmest conclusions can be drawn about the loss of the *eq*-apoMb AGH-core. Upon cold denaturation, previous microcalorimetry and intrinsic viscosity measurements indicate disruption of the *eq*-apoMb hydrophobic cores,[14] and small-angle X-ray scattering data[13] show an increase in protein size. The present experiments show that this globally monitored disruption is not limited to the CDEF domain but occurs also in the AGH-hydrophobic core. Our −8 °C NMR data show that nativelike tertiary interactions in the A-helix disappear at various locations between 2 and 17, unlike the acid-denatured state, which retains some interactions. An exactly parallel transition upon cold denaturation is also seen in the tryptophan side chain mobility by near-UV CD. Finally, the inner face of the A-helix becomes solvent exposed, leading to a red fluorescence shoulder.

While the CD, IR, NMR, and S2 fluorescence data all show this transition in lockstep below 3 °C, the S1 component shows hyperfluorescence with a different temperature dependence (Figure 8). We attribute this to a "pretransition" loosening of the core without significant solvent exposure. At lower temperatures, the *eq*-apoMb fluorescence finally decreases just as observed during complete acid or GuHCl denaturation in both *eq*- and *pc*-apoMb (Figure 9).[22,49,54,55,57] During acid denaturation of *pc*-apoMb, the hyperfluorescent state appears as a bona fide intermediate whose population can be varied by mutations.[22] In our cold-denaturation experiment, there is no evidence for a third state in any of the other measurements (e.g., CD). Hence we attribute the hyperfluorescence to a "pre-transition" loosening of the core. A true stabilized intermediate could arise under different conditions.

As a final point concerning the AGH-core, the I-state of *eq*-apoMb itself cold denatures below −3 °C as seen by CD and NMR (Figures 6 and 11). This behavior has been observed previously by small-angle X-ray scattering and near- and far-UV CD.[13] The *eq*-apoMb I-state is therefore not a likely structural model for cold denaturation at pH 5.9. In any case, it already has insufficient secondary structure (31%) to account for an intact AGH-core, unlike the I-state of *pc*-apoMb (41%), which has been shown by NMR to largely consist of an intact AGH-core, and whose CD is the only denatured state in Figure 6 compatible with an intact AGH-complex (40%). Cold denaturation is therefore nearly equally adept at dissolving the AGH-core in the I-state, where it is the only partially remaining hydrophobic core, as it is at doing so at pH 5.9. It should be noted that unlike the pH 5.9 case, the temperatures currently accessible by supercooling do not allow unambiguous assignment of the I-state cold denaturation to a cooperative two-state process.

Regarding nativelike structure in the GH-complex, the mobility of *eq*-apoMb tyrosine side chains in the middle of the GH-interface as monitored by near-UV CD appears to be unaffected by cold denaturation (Figure 6). While NMR data clearly show that tyrosine 146 in native *pc*-apoMb is in a fluctuating environment (but not in a coil),[17] Rischel and Poulsen have previously reported fluorescence data that indicates some structural rigidity in the GH-interface at residue 146 of native *eq*-apoMb.[49] It appears from the present data that such rigidity could be maintained even upon cold denaturation.

The G- and H-helices both have greater helical propensity than does the A-helix of *eq*-apoMb. Since the GH-subsequence is highly conserved between *eq*- and *pc*-apoMb, results about the latter are relevant to the discussion of *eq*-apoMb here. A 51-residue peptide corresponding to the entire GH-protein moiety from *pc*-apoMb[46] has been found to adopt helical structure at very low concentrations of TFE (10%). The authors found the hairpin turn at the bottom of the AGH-core to be intact even in absence of TFE.[47] Most of the helical conformation is still present in the middle of the H-helix.[46] Cooling should further increase the amount of GH-helical structure, in analogy with the behavior seen here for A-peptide in 50% TFE (Figure 3), for *pc*-apoMb H-helix,[43] and for many other peptides, which generally are stabilized by lower temperatures.[42,44] Finally, a previous study of mini-apoMb (residues 32−139 of *eq*-apoMb) shows that without the A- and B-helices, the protein still adopts an acid-intermediate conformation (pH 4.8) with almost the same helix content as the fully intact I-state.[68] This demonstrates that the GH-subdomain need not be in contact with the A-helix to attain some secondary and tertiary structure. It also indicates that most of the *eq*-apoMb CD signal of the I-state in Figure 6 is likely due to GH. It appears that many of the side chains of the GH-helices form a tightly packed "zipper", which is impervious to cold denaturation above −20 °C and indirectly stabilizes the helices.

In contrast to the GH-helices, there are several indications that the A-helix largely, if not completely, melts following disruption of the AGH-hydrophobic core. With the conservative assumption that BCDEF make no contribution to the helical fraction (f_H) in the cold-denatured state, f_H of cold-denatured *eq*-apoMb (31%, Figure 6) still accounts only for intact GH-helices. It lies below that of the *eq*-apoMb I-state, and well below f_H of the *pc*-apoMb I-state, known to consist mainly of

an intact A(B)GH-complex.[20] Global measures such as far-UV CD or IR can of course not assign helicity to specific regions. However, a considerable amount of GH-helix would have to dissolve to make room for an intact A-helix. The literature NMR[46] and fluorescence data,[49] as well as our near-UV CD data (Figure 7), provide no indication that the GH hairpin or center residues are in a coil state. Available data on the contrary suggest more GH-helix content at lower temperatures.

As discussed above, the core side of the A-helix becomes solvent-exposed upon cold denaturation (Figure 8). In particular, the NMR upfield data indicate either complete loss of the original structure or rapid equilibration between folded and unfolded states: the nativelike peaks decrease in intensity without broadening, presumably reappearing either at a random-coil or folded/unfolded averaged peak location. Loss of the AGH-core isolates the A-helix from the remainder of the protein. Without hydrophobic stabilization, the low helix propensity of A-peptide prevents it from forming helical structure in aqueous solution even at low temperature (Figure 3).

In a sense, hydrophobic interactions act as stabilizers of amphiphilic helices, inducing their formation much like addition of TFE. Upon cold denaturation, these hydrophobic interactions are weakened and helix formation in this state becomes more dependent on a segment's intrinsic helix propensity, which seems high for G and H but low for *eq*-A-helix. The A-helix either melts or undergoes conformational averaging between a nativelike helix and a conformation with residues 2−17 adopting statistical coil configurations, depending on the strength of residual nonspecific hydrophobic interactions in the absence of the AGH-core.

The idea of a nativelike GH tightly packed "zipper" without an AGH-core or a folded A-helix is not without precedent. As discussed above, DeSanctis et al. observed a mini-*eq*-apoMb I-state without the A- and B-helices, but with essentially the same helix content as a fully intact I-state. A resonance Raman study of Mb acid denaturation shows that a GH-complex could remain after the A-helix has been disrupted. (Chi, Z.; Asher, S. A. *Biochemistry*, in press). The I-state of *eq*-apoMb shows a significant spatial rearrangement of the A-helix tryptophan residues with respect to tyrosine 146,[49] indicating a weaker AGH-core than in *pc*-apoMb. The data on GH-peptide[46] further support the stability of GH independent of A.

On the other hand, many experiments show that the AGH-core acts as a single unit. The AGH-complex is clearly present in pH 5.9 *pc*-apoMb and *eq*-apoMb[16−18] and remains intact in several acid-intermediate states of *pc*-apoMb.[19−22] Stopped-flow hydrogen exchange experiments indicate that an intact AGH-core from *pc*-apoMb is a kinetic intermediate.[23] Molecular dynamics simulations of *pc*-apoMb in water show a fairly intact AGH-core at 85 °C, even at pH 4.2,[24] while molecular dynamics simulations of the heat-initiated unfolding of the peptide sequences of *pc*-Mb indicate that A-, G-, and H-helices are all similarly stable and, even individually, are the most stable regions of the protein.[69]

The answer to the question of why the AGH-core generally has been viewed as a single stable unit probably lies within the stability of the helices themselves, coupled with the fact that the other Mb-helices retain no structure in the acid intermediate.[20] Most previous studies were carried out with *pc*-apoMb, which does not show the same thermodynamic behavior as *eq*-apoMb. It has been known for some time that *pc*-Mb is about 15% more stable than *eq*-Mb.[28] Upon heme removal, *pc*-apoMb continues to be more stable. Upon acid denaturation, its CD spectrum shows about 6% more helix than that of *eq*-apoMb. Finally, its residues 3−18 have considerably higher helix-forming propensity (1.19) than those of *eq*-apoMb (1.06), indicating that *pc*-apoMb cannot be taken as a good model of *eq*-apoMb in discussions of the AGH-hydrophobic core.

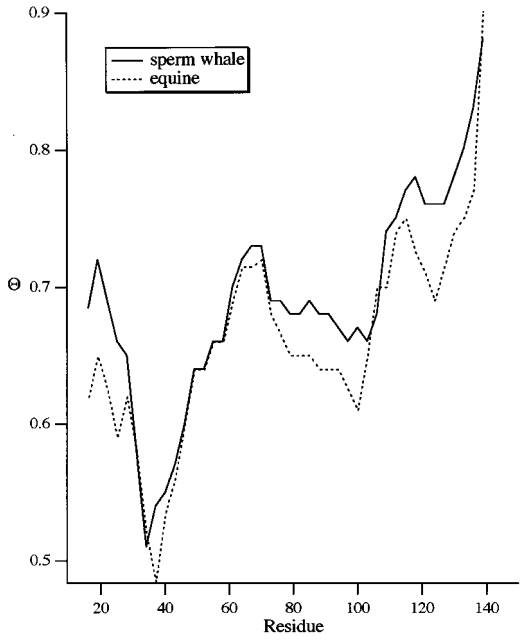

Figure 13. Folding-unit calculation from Panchenko et al.[70] done as described in the text. The calculation is not based on any a priori input data from apomyoglobins other than their sequences, yet it also shows the increased propensity for the A-helix in *pc*-apoMb to be part of a folding unit as compared to *eq*-apoMb. The GH-"zipper" is hierarchically the most stable structure, followed by the AGH-core.

The difference between the two molecules is also indicated by the folding-unit calculations of Panchenko et al. in Figure 13.[70] To show this difference the protein is cut at a certain residue. The resultant segments' sequences are then run through a set of protein structure templates, and the energy is calculated. A distribution of energies results. The difference in its average energy from that of the protein's native state (ΔE) and the variance of the distribution (δE) are then incorporated into two quantities, each called Θ (defined as $\Delta E/\delta E$), one for each of the two protein segments. The Θ in Figure 13 is the average of these two energy gap vs fluctuation stability criteria. The computed increased stability of the *pc*-apoMb A-helix and AGH-core corroborates the results from helical propensity calculations.

This discussion leads to the construction of an AGH-subdomain phase diagram shown in Figure 14. Upon cooling at pH 5.9, pretransition core-loosening is followed by cooperative disruption of the AGH-core and loss of the A-helix in the cold-denatured state. In another cooperative transition, lowering the pH produces an I-state with a less-defined AGH-core than that of *pc*-apoMb. This AGH-core also undergoes cold denaturation, although the cooperativity of the process remains untested. Upon lowering the pH to 2, the secondary and tertiary structures are almost fully disrupted. Heat denaturation leads to a state with only 10% remaining helicity at pH 5.9, although the mobility of AGH-core residues appears to be restricted, at least up to 35 °C.

In light of the current study, the previously obtained fast folding kinetics results can be understood in more detail.[6,8] The 3.5−17-μs quenching phase (depending on solvent viscosity) is due to formation of a nativelike AGH-core from the nascent A-helix and the preexisting GH-zipper. The CDEF-helices act

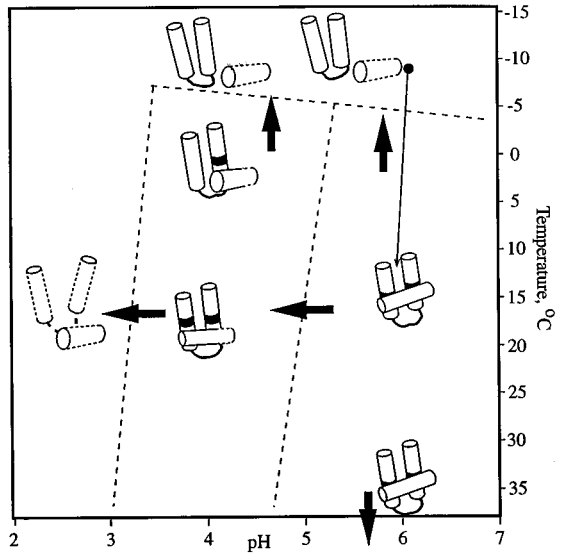

Figure 14. Temperature−pH phase diagram for *eq*-apoMb denaturation. Dissolved helices are indicated by dashed lines, cooperative phase transitions by fat arrows, and transition midpoints by dashed zones. A typical fast T-jump experiment is indicated by the narrow arrow.

as a nearly random-coil tether of length 60−70 residues, for which a diffusion-limited core formation rate of 3.5 μs appears reasonable.

In terms of a free energy landscape, the core formation rate in such a short time indicates a relatively small ratio of landscape fluctuations to the downhill driving force, at least at the top of the funnel. This would imply a type 0, or type 1 close to 0, scenario for the earliest folding events.[71] It remains to be seen if the experimental time scale would be lengthened significantly by a mutation that disrupts the GH-zipper, and if A, G, and H would then condense simultaneously or in a U → GH → AGH temporal sequence.

When AGH-core formation is viewed as a collision process, the fast folding experiment measures a "half-collision" event, since GH is already preformed. Core formation proceeds faster if secondary structure in one of the two colliding domains is already preformed. In terms of a collision−diffusion model, preformation of GH implies that the rate depends on $\beta^{1/2}$ rather than β itself. However, the experimental rate on the order of 0.1−0.3 μs^{-1} still implies a value of β close to unity,[72] indicating rapid formation of helical structure. This is compatible with the idea proposed above that nonspecific or nativelike hydrophobic contacts can facilitate the formation of amphiphilic helices and stabilize them. They could also be responsible for residual A-helix in the absence of the AGH-core.

If nonspecific tertiary contacts, rather than nativelike contacts, are sufficient to stabilize amphiphilic helices such as the A-helix, the time scale of refolding will be dictated by shorter chain lengths than the 80 residues separating A from GH, leading to times in the 0.2−1-μs range. It remains to be seen from further fast measurements whether the 0.25-μs phase observed in the fast folding experiment is due to such a local collapse/helix formation process or has another explanation. In the former case, the two phases would be an example of a nonspecific collapse−secondary structure formation−nativelike collapse sequence during the early folding steps.

Acknowledgment. The authors thank Profs. S. Asher, R. Baldwin, J. Dyson, T. Haymet, Z. Schulten, and P. Wolynes for helpful discussions and comments. Steady-state fluorescence and CD measurements were performed at the University of Illinois Laboratory of Fluorescence Dynamics. This work was supported by NSF Grant CHE 94-57970 and the David and Lucile Packard Foundation. M.G. was a Sloan Fellow and Cottrell Scholar while this work was carried out.

References and Notes

(1) Privalov, P. L.; Griko, Y.; Venyaminov, S.; Kutyshenko, V. P. *J. Mol. Biol.* **1986**, *190*, 487.
(2) Griko, Y. V.; Privalov, R. L.; Sturtevant, J. M.; Vanyaminov, S. Y. *Proc. Natl. Acad. Sci. U.S.A.* **1988**, *85*, 3343.
(3) Privalov, P. L. *Crit. Rev. Biochem. Mol. Bio.* **1990**, *25*, 281.
(4) Gast, K.; Damaschun, G.; Damaschun, H.; Misselqitz, R.; Zirwer, D. *Biochemistry* **1993**, *32*, 7747.
(5) Huang, G. S.; Oas, T. G. *Biochemistry* **1996**, *35*, 6173.
(6) Ballew, R. M.; Sabelko, J.; Gruebele, M. *Proc. Natl. Acad. Sci. U.S.A.* **1996**, *93*, 5759.
(7) Nölting, B.; Golbik, R.; Neira, J. L.; Soler-Gonzalez, A. S.; Schreiber, G.; Fersht, A. R. *Proc. Natl. Acad. Sci. U.S.A.* **1997**, *94*, 826.
(8) Ballew, R. M.; Sabelko, J. and Gruebele, M. *Nat. Struct. Biol.* **1996**, *3*, 923.
(9) Hagen, S. J.; Hofrichter, J.; Szabo, A. and Eaton, W. A. *Proc. Natl. Acad. Sci. U.S.A.* **1996**, *93*, 11615.
(10) Zhang, J.; Peng, X.; Jonas, A.; Jonas, J. *Biochemistry* **1995**, *34*, 8631.
(11) Nash, D. P. Ph.D. Thesis, University of Illinois, 1997.
(12) Petrescu, A.; Receveur, V.; Calmettes, P.; Durand, D.; Desmadril, M.; Roux, B.; Smith, J. C. *Biophys. J.* **1997**, *72*, 335.
(13) Nishii, I.; Kataoka, M.; Tokunaga, F.; Goto, Y. *Biochemistry* **1994**, *33*, 4903.
(14) Griko, Y. V.; Privalov, P. L.; Venyaminov, S. Y.; Kutyshenko, V. P. *J. Mol. Biol.* **1988**, *220*, 127.
(15) Cocco, M. J.; Lecomte, J. T. J. *Biochemistry* **1990**, *29*, 11067.
(16) Lecomte, J. T. J.; Kao, Y.; Cocco, M. J. *Proteins: Struct., Funct., Genet.* **1996**, *25*, 267.
(17) Eliezer, D.; Wright, P. E. *J. Mol. Biol.* **1996**, *263*, 531.
(18) Yamamoto, Y. *Eur. J. Biochem.* **1997**, *243*, 292.
(19) Loh, S.; Kay, M.; Baldwin, R. *Proc. Natl. Acad. Sci. U.S.A.* **1995**, *92*, 5446.
(20) Hughson, F.; Wright, P.; Baldwin, R. *Science* **1990**, *249*, 1544.
(21) Hughson, F.; Barrik, D.; Baldwin, R. *Biochemistry* **1991**, *30*, 4113.
(22) Kay, M.; Baldwin, R. *Nat. Struct. Biol.* **1996**, *3*, 439.
(23) Jennings, P.; Wright, P. *Science* **1993**, *262*, 892.
(24) Tirado-Rives, J.; Jorgensen, W. L. *Biochemistry* **1993**, *32*, 4175.
(25) Fanelli, A. R.; Antonini, E.; Caputo, A. *Methods Enzymol.* **1958**, *30*, 608.
(26) Edelhoch, H. *Biochemistry* **1967**, *6*, 1948.
(27) Crumpton, M. J.; Polson, A. *J. Mol. Biol.* **1965**, 11, 722.
(28) Puett, D. *J. Biol. Chem.* **1973**, *248*, 4623.
(29) Antonini, M.; Brunori, E. *Hemoglobin and Myoglobin and Their Reactions and Ligands*; North-Holland Publishers: Amsterdam, 1971.
(30) Sligar, S. G.; Springer, B. A. *Proc. Natl. Acad. Sci. U.S.A.* **1987**, *84*, 8961.
(31) Silow, M.; Oliveberg, M. *Proc. Natl. Acad. Sci. U.S.A.* **1997**, *94*, 6084.
(32) Creighton, T. E. *Proteins*; W. H. Freeman: New York, 1993.
(33) Alonso, D. O. V.; Dill, K. A.; Stigter, D. *Biopolymers* **1991**, *31*, 1631.
(34) Barrick, D.; Hughson, F. M.; Baldwin, R. L. *J. Mol. Biol.* **1994**, *237*, 588.
(35) Kiefhaber, T.; Baldwin, R. L. *J. Mol. Biol.* **1995**, *252*, 122.
(36) Reymond, M. T.; Merutka, G.; Dyson, H. J.; Wright, P. E. *Protein Sci.* **1997**, *6*, 706.
(37) Williams, R. W.; Chang, A.; Juretic, D.; Loughran, S. *Biochim. Biophys. Acta* **1987**, *916*, 200.
(38) Blaber, M.; Zhang, X.; Matthews, B. W. *Science* **1993**, *260*, 1637.
(39) O'Neil, K. T.; DeGrado, W. F. *Science* **1990**, *250*, 646.
(40) Woody, R. W. In *Circular Dichroism and the Conformational Analysis of Biomolecules;* Fasman, G. D., Ed.; Plenum Press: New York, 1996.
(41) Yang, J. T.; Wu, C. C. and Martinez, H. M. *Methods Enzymol.* **1986**, *130*, 208.
(42) Anderson, N. H.; Cort, J. R.; Liu, Z.; Sjoberg, S. J.; Tong, H. *J. Am. Chem. Soc.* **1996**, *118*, 10309.
(43) Waltho, J. P.; Feher, V. A.; Merutka, G.; Dyson, H. J.; Wright, P. E. *Biochemistry* **1993**, *32*, 6337.
(44) Bierzynski, A.; Kim, P. S.; Baldwin, R. L. *Proc. Natl. Acad. Sci. U.S.A.* **1982**, *79*, 2470.
(45) Chakrabartty, A.; Baldwin, R. L. *Adv. Protein Chem.* **1995**, *46*, 141.
(46) Shin, H.; Merutka, G.; Waltho, J. P.; Tennant, L. L.; Dyson, H. J.; Wright, P. E. *Biochemistry* **1993**, *32*, 6356.

(47) Shin, H.; Merutka, G.; Waltho, J. P.; Wright, P. E.; Dyson, H. J. *Biochemistry* **1993**, *32*, 6348.
(48) Johnson, W. C. J. *Annu. Rev. Biophys. Biophys. Chem.* **1988**, *17*, 145.
(49) Rischel, C.; Poulsen, F. M. *FEBS Lett.* **1995**, *374*, 105.
(50) Venyaminov, S. Y.; Yang, J. T. In *Circular Dichroism and the Conformational Analysis of Biomolecules;* Fasman, G. D., Ed.; Plenum Press: New York, 1996.
(51) Evans, S. V.; Brayer, G. D. *J. Mol. Biol.* **1990**, *213*, 885.
(52) Woody, R. W.; Dunker, A. K. In *Circular Dichroism and the Conformational Analysis of Biomolecules;* Fasman, G. D., Ed.; Plenum Press: New York, 1996.
(53) Gast, K.; Damaschun, H.; Misselwitz, R.; Müller-Frohne, M.; Zirwer, D.; Damaschun, G. *Eur. Biophys. J.* **1994**, *23*, 297.
(54) Postnikova, G. B.; Komarov, Y. E.; Jumakova, E. M. *Eur. J. Biochem.* **1991**, *198*, 223.
(55) Postnikova, G. B.; Komarov, Y. E. *Mol. Biol.* **1990**, *24*, 757.
(56) Jamin, M.; Baldwin, R. *Nat. Struct. Biol.* **1996**, *3*, 613.
(57) Ramsay, G.; Ionescu, R.; Eftink, M. R. *Biophys. J.* **1995**, *69*, 701.
(58) Press, W. H.; Teukolsky, S. A.; Vetterling, W. T.; Flannery, B. P. *Numerical Recipes in Fortran: The Art of Scientific Computing*; Cambridge University Press: Cambridge, 1992.
(59) Gilst, M. v.; Tang, C.; Roth, A.; Hudson, B. *J. Fluoresc.* **1994**, *4*, 203.
(60) Steiner, R. F.; Kirby, E. P. *J. Phys. Chem.* **1969**, *73*, 4130.
(61) Susi, H. *Methods Enzymol.* **1971**, *22*, 455.
(62) Gilmanshin, R.; Williams, S.; Callender, R. H.; Woodruff, W. H.; Dyer, R. B. *Proc. Natl. Acad. Sci. U.S.A.* **1997**, *94*, 3709.
(63) Bene, J. E. D.; Shavitt, I. In *Molecular Interactions;* Scheiner, S., Ed.; John Wiley & Sons Ltd: New York, 1997.
(64) Wong, K.; Freund, S. M. V.; Fersht, A. R. *J. Mol. Biol.* **1996**, *259*, 805.
(65) Buck, M.; Radford, S. E.; Dobson, C. M. *Biochemistry* **1993**, *32*, 669.
(66) Cocco, M. J. Ph.D. Thesis, Pennsylvania State University, 1994.
(67) Franks, F. *Adv. Protein Chem.* **1995**, *46*, 105.
(68) DeSanctis, G.; Ascoli, F.; Brunori, M. *Proc. Natl. Acad. Sci. U.S.A.* **1994**, *91*, 11507.
(69) Hirst, D.; Brooks, C. *Biochemistry* **1995**, *34*, 7614.
(70) Panchenko, A. R.; Luthey-Schulten, Z.; Wolynes, P. G. *Proc. Natl. Acad. Sci. U.S.A.* **1996**, *93*, 2008.
(71) Bryngelson, J. D.; Onuchic, J. N.; Socci, N. D.; Wolynes, P. G. *Proteins: Struct., Funct., Genet.* **1995**, *21*, 167.
(72) Karplus, M.; Weaver, D. L. *Protein Sci.* **1994**, *3*, 650.
(73) Humphrey, W. F.; Dalke, A.; Schulten, K. *J. Mol. Graphics* **1996**, *14*, 33.